Journal of Alloys and Compounds

Facile Synthesis and Efficient Photoelectrochemical Reaction of WO3/WS2 Core–Shell Nanorods Utilizing WO3•0.33H2O Phase

--Manuscript Draft--

Manuscript Number:	
Article Type:	Full Length Article
Keywords:	WO3; WS2; photoelectrocatalysis; 2D nanostructures; nanorods; hydrothermal synthesis
Corresponding Author:	Eui-Tae Kim, Ph.D. Chungnam National University Daejeon, KOREA, REPUBLIC OF
First Author:	Dong-Bum Seo
Order of Authors:	Dong-Bum Seo
	Soomin Yoo
	Viet Dongquoc, Ph.D.
	Tran Nam Trung, Ph.D.
	Eui-Tae Kim, Ph.D.
Abstract:	One-dimensional (1D) WO3/two-dimensional (2D) WS2 heterojunction nanostructures are of great interest in various photoelectrochemical (PEC) and electrochemical applications. In this study, we introduced a simple and effective route to synthesize 2D WS2 shell layer on WO3 nanorods by utilizing WO3•0.33H2O phase. The formation of WO3•0.33H2O nanorods was critically affected by hydrothermal reaction temperature. The WO3•0.33H2O phase was preferentially transformed into hexagonal WO3 and 2D WS2 through oxidation and sulfurization at 450 °C, respectively. The 2D WS2 shell layer was more favorably formed on WO3 nanorods, which were synthesized at 180 °C and possessed a significant amount of WO3•0.33H2O phase (referred to as W-180), than on WO3 nanorods with predominant monoclinic WO3 phase, which were synthesized at 200 °C (referred to as W-200). Thus, the WO3/WS2 core–shell nanorods from W-180 exhibited significantly enhanced PEC performance because of the improved charge transfer properties attributed to the advantageous heterojunction effect of 1D WO3/2D WS2. The new synthesis route from WO3•0.33H2O phase to 2D WS2 can be applied to synthesize various WO3/2D WS2 heterojunction nanostructures, such as thin films, nanoparticles, and nanorods.
Suggested Reviewers:	Paul O'Brien, Ph.D. Profesor, The University of Manchester paul.o'brien@manchester.ac.uk Strong research background on the synthesis and PEC applications of nanomaterials
	Simelys Hernández, Ph.D. Istituto Italiano di Tecnologia simelys.hernandez@iit.it Strong research background on the synthesis and PEC applications of nanomaterials
	Junhong Park, Ph.D. Profesor, Gyeongsang National University yakte@gnu.ac.kr Active research on the synthesis and applications of 2D nanomaterials.
Opposed Reviewers:	
Order of Authors (with Contributor Roles):	Dong-Bum Seo
	Soomin Yoo
	Viet Dongquoc, Ph.D.
	Tran Nam Trung, Ph.D.

	Eui-Tae Kim, Ph.D.

DEPARTMENT OF MATERIALS SCIENCE & ENGINEERING
CHUNGNAM NATIONAL UNIVERSITY

99 DAEHAK-RO, DAEJEON 34134, KOREA
Tel. +82-42-821-6631 Fax. +82-42-822-5850 http://mateng.cnu.ac.kr

June 6, 2021

Dear Editor,

Please find enclosed our manuscript entitled "Facile Synthesis and Efficient Photoelectrochemical Reaction of WO_3/WS_2 Core–Shell Nanorods Utilizing $WO_3 \cdot 0.33H_2O$ Phase", which we would like you to consider for publication of an *Original Article* in *Journal of Alloys and Compounds*.

One-dimensional (1D) WO_3/two-dimensional (2D) WS_2 heterojunction nanostructures are of great interest in various photoelectrochemical (PEC) and electrochemical applications. In this study, we introduce a facile and effective route to synthesize 1D WO_3/2D WS_2 core–shell nanorods by utilizing $WO_3 \cdot 0.33H_2O$ phase. We show that the $WO_3 \cdot 0.33H_2O$ can be a desirable intermediate structure to form 2D WS_2 shell layer on WO_3 nanorods because it can create more reduced oxidation states of WO_3 from 6+ to 5+ by easily releasing H_2O through thermal sulfurization. The created oxygen vacancies are filled up by S species and form thermodynamically stable WS_2. The WO_3/WS_2 core–shell nanorods exhibit significantly improved PEC performance because of their enhanced charge transfer properties along the heterojunction. The new transformation route from $WO_3 \cdot 0.33H_2O$ phase to 2D WS_2 can be applied to synthesize various types of heterojunction WO_3/2D WS_2, such as films, nanoparticles, and nanowires, for PEC and electrochemistry applications.

I look forward to hearing from you at your earliest convenience.
Thank you.

Sincerely,

Eui-Tae Kim, Ph.D.
Professor
Department of Materials Science & Engineering
Chungnam National University
Daejeon 34134, Korea
E-mail: etkim@cnu.ac.kr
Tel: +82 42-821-5895

Prime Novelty Statement

Facile Synthesis and Efficient Photoelectrochemical Reaction of WO_3/WS_2 Core–Shell Nanorods Utilizing $WO_3 \cdot 0.33H_2O$ Phase

One-dimensional (1D) WO_3/two-dimensional (2D) WS_2 heterojunction nanostructures are of great interest in various photoelectrochemical (PEC) and electrochemical applications. In this study, we introduce a facile and effective route to synthesize 1D WO_3/2D WS_2 core–shell nanorods by utilizing $WO_3 \cdot 0.33H_2O$ phase. We show that the $WO_3 \cdot 0.33H_2O$ can be a desirable intermediate structure to form 2D WS_2 shell layer on WO_3 nanorods because it can create more reduced oxidation states of WO_3 from 6+ to 5+ by easily releasing H_2O through thermal sulfurization. The created oxygen vacancies are filled up by S species and form thermodynamically stable WS_2. The WO_3/WS_2 core–shell nanorods exhibit significantly improved PEC performance because of their enhanced charge transfer properties along the heterojunction. The new transformation route from $WO_3 \cdot 0.33H_2O$ phase to 2D WS_2 can be applied to synthesize various types of heterojunction WO_3/2D WS_2, such as films, nanoparticles, and nanowires, for PEC and electrochemistry applications.

Facile Synthesis and Efficient Photoelectrochemical Reaction of WO_3/WS_2 Core–Shell Nanorods Utilizing $WO_3 \cdot 0.33H_2O$ Phase

Dong-Bum Seo, Soomin Yoo, Viet Dongquoc, Tran Nam Trung, and Eui-Tae Kim*

Department of Materials Science & Engineering, Chungnam National University, Daejeon 305-764, Republic of Korea

* Correspondence: etkim@cnu.ac.kr

One-dimensional (1D) WO_3/two-dimensional (2D) WS_2 heterojunction nanostructures are of great interest in various photoelectrochemical (PEC) and electrochemical applications. In this study, we introduced a simple and effective route to synthesize 2D WS_2 shell layer on WO_3 nanorods by utilizing $WO_3 \cdot 0.33H_2O$ phase. The formation of $WO_3 \cdot 0.33H_2O$ nanorods was critically affected by hydrothermal reaction temperature. The $WO_3 \cdot 0.33H_2O$ phase was preferentially transformed into hexagonal WO_3 and 2D WS_2 through oxidation and sulfurization at 450 ℃, respectively. The 2D WS_2 shell layer was more favorably formed on WO_3 nanorods, which were synthesized at 180 ℃ and possessed a significant amount of $WO_3 \cdot 0.33H_2O$ phase (referred to as W-180), than on WO_3 nanorods with predominant monoclinic WO_3 phase, which were synthesized at 200 ℃ (referred to as W-200). Thus, the WO_3/WS_2 core–shell nanorods from W-180 exhibited significantly enhanced PEC performance because of the improved charge transfer properties attributed to the advantageous heterojunction effect of 1D WO_3/2D WS_2. The new synthesis route from $WO_3 \cdot 0.33H_2O$ phase to 2D WS_2 can be applied to synthesize various WO_3/2D WS_2 heterojunction nanostructures, such as thin films, nanoparticles, and nanorods.

Keywords: WO_3, WS_2, photoelectrocatalysis, 2D nanostructures, nanorods, hydrothermal synthesis

1. Introduction

Tungsten oxide (WO_3) has been extensively studied for photoelectrochemical (PEC) water splitting because of its non-toxicity, superior stability in acidic solutions, and relatively good charge-carrier transport property [1]. Nevertheless, the PEC performance of WO_3- based photoelectrodes is limited by several issues, such as the weak absorption of visible light with bandgap of 2.4–2.8 eV and short hole diffusion lengths. To resolve these problems and enhance the PEC activity, several strategies are utilized, including crystalline variation, doping, morphology control, and heterostructure with other semiconductors [1–4]. In particular, one-dimensional (1D) WO_3/two-dimensional (2D) WS_2 core–shell heterostructures has recently attracted considerable attention for PEC electrode applications due to their unique structural and electrical advantages. 1D WO_3 nanostructures provide a high specific surface area, a fast transport path along 1D architecture and short diffusion paths to the solid/aqueous solution interface. 2D layered WS_2 nanostructures exhibit high catalytic activity and tunable bandgaps for efficient visible-light absorption [5,6].

The synthesis of 1D WO_3/2D WS_2 core–shell heterostructures via the sulfurization of WO_3 nanowires/rods under various sulfur environment has recently been reported. Choudhary et al. prepared heterostructures by growing WO_3 nanowires on W foil followed by thermal sulfurization [7]. Kumar et al. fabricated heterostructures sulfurizing WO_3 nanorods on glass under H_2S/Ar plasma [8]. Most 1D WO_3/2D WS_2 core–shell synthesis approaches have commonly been based on the sulfurization of stoichiometric WO_3. However, monoclinic WO_3 comprises corner-sharing WO_6 octahedra, and its tungsten–oxygen bond energy (672 ± 41.8 kJ/mol) [9] is so high that oxygen–sulfur exchange reaction can occur at high temperature. Moreover, the exchange reaction requires a considerable amount of oxygen vacancies in WO_3. Van der Vlies et al. reported that sulfur can only be incorporated into significantly reduced WO_{3-x}, of which about 20% of tungsten centers are reduced from 6+ to 5+ oxidation state [9,10]. In general, WO_3 can be reduced to substoichiometric WO_{3-x} by producing

thermodynamically favored H_2O from intermediate H_xWO_3 under H_2S environment. Thus, $WO_3 \cdot 0.33H_2O$ nanostructures, an as-synthesized form of hydrothermal reaction, are one of the promising candidates to facilitate the formation of 2D layered WS_2.

Herein, we report a facile and efficient approach for synthesizing 1D WO_3/2D WS_2 core–shell heterostructures by direct sulfurization treatment of hydrothermally synthesized $WO_3 \cdot 0.33H_2O$ nanorods. The $WO_3 \cdot 0.33H_2O$ can be a desirable intermediate structure to form 2D WS_2 shell layer on WO_3 nanorods because oxygen vacancies can be efficiently formed by releasing H_2O during thermal sulfurization. In addition, we show that the hydrothermal reaction temperature of $WO_3 \cdot 0.33H_2O$ nanorods significantly affects the synthesis and PEC properties of 1D WO_3/2D WS_2 core–shell nanorods by determining the structural phases and relative volume ratio of $WO_3 \cdot 0.33H_2O$.

2. Experimental

Nanorods with a mixture of $WO_3 \cdot 0.33H_2O$ and WO_3 phases were synthesized on fluorine-doped tin oxide (FTO) glass substrates via a hydrothermal reaction in a Teflon-lined autoclave. The preparation process was as follows: Sodium tungstate dihydrate ($Na_2WO_4 \cdot 2H_2O$) and potassium oxalate ($K_2C_2O_4 \cdot H_2O$) were used as W and S sources, respectively. First, 2.4 g of $Na_2WO_4 \cdot 2H_2O$ and 0.2 g of $K_2C_2O_4 \cdot H_2O$ were dissolved in 90 mL of deionized (DI) water under stirring. After stirring for 6 h, 15 mL of 2 M concentrated hydrochloric acid was added to adjust the pH level to an acidic environment. After stirring for another 10 min, the prepared solution was transferred into a sealed autoclave and maintained at 180 °C and 200 °C for 12 h. After cooling down to room temperature, the as-obtained samples were washed with ethanol and DI water and dried at 60 °C in air. Subsequently, the samples were annealed at 450 °C for 1 h under O_2 and H_2S gas atmospheres, to obtain stoichiometric WO_3 and WO_3/WS_2 core–shell nanorods, respectively (Fig. 1).

The morphology and microstructure of nanorods were characterized via scanning electron microscopy (SEM, Hitachi S-4800) and transmission electron microscopy (TEM, Tecnai G^2 F30 S-Twin). The crystal structure was examined by TEM, X-ray diffraction (XRD, Bruker AXS D8 Discover), and micro-Raman spectroscopy using an excitation band of 532 nm and a charge-coupled device detector. PEC cells were fabricated on 1×2 cm^2 FTO glass substrates. PEC characterization was performed using a three-electrode system and an electrochemical analyzer (potentiostat/galvanostat 263A). A Pt plate and KCl-saturated calomel (Hg/Hg_2Cl_2) were used as counter and reference electrodes, respectively. The electrolyte solution comprised 0.3 M KH_2PO_4. The light source used was a 150 W Xe arc lamp that delivered an intensity of 100 mW/cm^2 of simulated AM 1.5 G irradiation. The current–voltage characteristics were recorded using a sourcemeter (Keithley 2400). Electrochemical impedance spectroscopy (EIS) measurement was performed under constant light illumination (100 mW/cm^2) at a bias of 0.6 V while varying the AC frequency from 100 kHz to 100 mHz.

3. Results and Discussion

Figures 2(a) and 2(b) show the SEM images of nanorods on FTO substrates synthesized at 180 °C and 200 °C, respectively (hereinafter referred to as W-180 and W-200, respectively). Most nanorods of W-180 appeared as long rectangular bars with a length of ~3–4 μm and width of ~300–500 nm. W-200 showed slightly longer and thicker nanorods than W-180. The length and width of W-200 were ~4–5 μm and ~400–600 nm, respectively. The W-200 nanorods exhibited well-developed rectangular facets, indicating that the nanorods were more crystallized at 200 °C. W-200 also possessed three-dimensional bricks, the formation of which can be attributed to Ostwald ripening [11]. After oxidation and sulfurization at 450 °C, the morphology of nanorods was not significantly changed (Figs. 2(c)–2(f)).

The XRD study clearly distinguished the crystal structure difference between W-180 and W-200 (Figs. 3(a) and 3(b), respectively). W-180 possessed a mixed structure of orthorhombic $WO_3 \cdot 0.33H_2O$ (JCPDS no. JCPDS-72-0199) and monoclinic WO_3 (JCPDS no. JCPDS-72-0677), and their relative XRD intensities were comparable to each other. By contrast, W-200 showed predominant peaks of monoclinic WO_3 with minor peaks of orthorhombic $WO_3 \cdot 0.33H_2O$. When W-180 and W-200 were oxidized at 450 °C (hereinafter referred to as WO-180 and WO-200, respectively), the hexagonal $WO_3 \cdot 0.33H_2O$ structure disappeared, but a new hexagonal WO_3 appeared. The presence of hexagonal WO_3 was clearly confirmed by the peaks at 14.0° and 22.8° of 2θ, corresponding to its (100) and (001) crystal plane (JCPDS no. 75-2187). For WO-180, the relative intensities of monoclinic WO_3 and hexagonal WO_3 were comparable to each other. On the other hand, WO-200 showed predominant peaks of monoclinic WO_3 with minor peaks of hexagonal WO_3. These results indicate that $WO_3 \cdot 0.33H_2O$ of as-synthesized samples is preferentially transformed to hexagonal WO_3 via oxidation. When W-180 and W-200 were sulfurized at 450 °C (hereinafter referred to as WOS-180 and WOS-200, respectively), a new peak appeared at 14.3° of 2θ, corresponding to the (002) crystal plane of hexagonal WS_2 (JCPDS no. 08-0237). WOS-180 exhibited relatively strong peaks of hexagonal WS_2 and WO_3, whereas WOS-200 showed predominant peaks of monoclinic WO_3 with minor peaks of hexagonal WS_2 and WO_3. The strong correlation of relative peak intensities of hexagonal WS_2 phase of sulfurized samples and $WO_3 \cdot 0.33H_2O$ phase in as-synthesized samples suggests that the presence of $WO_3 \cdot 0.33H_2O$ phase significantly promoted the formation of hexagonal WS_2 through sulfurization. The sulfurization synthesis of 2D layered WS_2 from WO_3 is generally known as a two-step process: i) the formation of substoichiometric WO_{3-x} and ii) the conversion of WO_{3-x} into WS_2 by filling up of oxygen vacancies by S species [8, 9]. Compared with stoichiometric WO_3, $WO_3 \cdot 0.33H_2O$ can create more reduced oxidation states of WO_3 from 6+ to 5+ by easily releasing H_2O through thermal sulfurization. The created oxygen vacancies can be filled up by S species and form thermodynamically stable WS_2 [8].

The oxygen–sulfur exchange reaction can be further facilitated by the defected sites and dangling bonds of $WO_3 \cdot 0.33H_2O$.

To further investigate the crystal structures of the oxidized and sulfurized samples, a micro-Raman spectroscopy study was carried out. Figure 4 shows the Raman spectra of WO-180, WO-200, WOS-180, and WOS-200. All samples exhibited the peaks around 275, 328, 720, and 809 cm^{-1}, corresponding to monoclinic WO_3 [8,12]. The first two peaks are attributed to the bending vibration of W–O–W [δ(W–O–W)], while the latter two peaks are related to the stretching vibration [ν(O–W–O)] of WO_3 [12–14]. WO-180 showed other shoulder peaks at 252 and 690 cm^{-1} (Fig. 4(a)), which correspond to hexagonal WO_3 [14]. By contrast, WO-200 exhibited only strong peaks of monoclinic WO_3 without distinguishable shoulder peaks. However, the Raman peaks at 275 and 720 cm^{-1} were not a perfect Gaussian shape, implying that a small volume of hexagonal WO_3 is present. WOS-180 and WOS-200 showed extra peaks at 353 and 417 cm^{-1}, corresponding to the E^1_{2g} and A_{1g} modes of 2D WS_2 (Fig. 3(b)). The E^1_{2g} and A_{1g} modes can be attributed to the in-plane vibration of W and S atoms and the out-of-plane vibration of S atoms, respectively [15]. Clearly, WOS-180 exhibited significantly stronger relative peak intensity of WS_2 to WO_3 than WOS-200, which is consistent with the XRD results.

The microstructures of WO-200 and WSO-200 were investigated using TEM. Figure 5(a) shows the TEM images of a typical nanorod of WO-200. The high-resolution TEM (HRTEM) image exhibited an interplanar distance of 0.38 nm, which is consistent with the (002) crystal plane distance of WO_3 [2]. The energy-dispersive X-ray spectroscopy (EDS) elemental mapping showed a homogeneous distribution of W and O elements throughout WO_3 nanorods (Fig. 5(b)). The formation of 1D WO_3/2D WS_2 core–shell nanorods through sulfurization was confirmed by TEM images, as shown in Fig. 5(c). The HRTEM image of WSO-200 showed that 2D layered WS_2 was formed on the WO_3 nanorod surface. The shell layer comprised ~10–15 layers with an interlayer spacing of 0.63 nm, corresponding to that

of 2D WS_2 [8]. The EDS elemental mapping confirmed that 2D WS_2 completely covered the whole surface of WO_3 nanorods (Fig. 5(d)).

The PEC activities of the oxidized and sulfurized nanorods were evaluated by recording the linear sweep voltammograms in the dark and under simulated AM 1.5 G illumination. The photocurrent density of WO-180 was lower than that of WO-200, whereas their dark current densities were comparable to each other (Fig. 6(a)). The catalytic properties of WO_3 have been reported to be manipulated by its phased transformation [16,17]. WO-200 with predominant monoclinic phase is favorable for PEC activity because the monoclinic phase can possess more oxygen vacancies than other phases [18]. Oxygen vacancies reduce tungsten centers from 6+ to 5+, resulting in enhanced photoactivity for O_2 production [19]. The PEC performance of WO_3 nanorods was significantly improved by the formation of WO_3/WS_2 core–shell nanorod structures (Fig.6(b)). Interestingly, unlike the WO_3 nanorod samples (WO-180 vs. WO-200), WSO-180 exhibited higher photocurrent densities than WSO-200 (Fig. 6(b)). The WO_3/WS_2 core–shell nanorods are known to form a staggered (type II) heterojunction as shown in Fig. 6(c) [8]. As a result, the heterojunction of WO_3/WS_2 can not only efficiently separate photogenerated electron–hole pairs, but also effectively transport electrons and holes into cathode and anode for hydrogen- and oxygen-evolution reactions, respectively. Therefore, being able to form well-developed 2D WS_2 on WO_3 nanorods easily, WSO-180 can be beneficial to achieve the highest PEC activity.

An EIS study was conducted to understand the charge transport properties of WO_3 and WO_3/WS_2 core–shell nanorods. Figures 7(a) and 7(b) show the Nyquist plots of EIS under illumination and in the dark, respectively. The Nyquist plots were fitted using a simplified Randles circuit (inset of Fig. 7(a)), which consists of the charge transfer resistance (R_{ct}), solution resistance (R_s), constant phase element (Q), and diffusion of species in the electrolyte solution represented by the Warburg impedance (W). WO-180 showed the largest radius of the EIS semicircle, indicating the highest charge transfer

resistance under illumination (R_{ct} (photo) ~ 15.9 kΩ), whereas WO-200 possessed an R_{ct} (photo) value of ~11.2 kΩ. The charge transfer properties of WO_3 nanorods were significantly improved by the formation of WO_3/WS_2 core–shell structures. The R_{ct} (photo) values of WSO-180 and WSO-200 were ~6.4 and ~8.2 kΩ, respectively, suggesting that the heterojunction of WO_3/WS_2 is highly effective for the separation and transportation of electrons and holes. In the dark, WO_3/WS_2 core–shell nanorods also exhibited significantly smaller radii than WO_3 nanorod samples (Fig. 7(b)). Notably, WSO-180 possessed the smallest R_{ct} (photo) value because it had well-developed 2D WS_2 shell layers on WO_3 nanorods.

4. Conclusion

We introduced a facile and effective route to synthesize 1D WO_3/2D WS_2 core–shell nanorods by utilizing $WO_3 \cdot 0.33H_2O$ phase, which was preferentially transformed into hexagonal WO_3 and 2D WS_2 through oxidation and sulfurization at 450 ℃, respectively. The 2D WS_2 shell layer was more favorably formed on W-180 nanorods, possessing a significant amount of $WO_3 \cdot 0.33H_2O$ phase, than on W-200 nanorods. For oxidized WO_3 nanorods, WO-200 exhibited better PEC performance than WO-180 because the dominant monoclinic phase of WO-200 was more beneficial for PEC reactions than the mixed monoclinic and hexagonal phases of WO-180. By contrast, the PEC performance of WSO-180 was superior to that of WSO-200 because of its significantly decreased charge transfer resistance. The enhanced charge transfer property of WSO-180 can be attributed to the advantageous heterojunction effect of 1D WO_3/2D WS_2. The new transformation route from $WO_3 \cdot 0.33H_2O$ phase to 2D WS_2 can be applied to synthesize various types of heterojunction WO_3/2D WS_2, such as films, nanoparticles, and nanowires, for PEC and electrochemistry applications.

Acknowledgements

This work was supported by the National Research Foundation of Korea (NRF) grants funded by the Korea government (MSIT) (2021R1A2C1006241 and 2020R1A4A4079397) and the Ministry of Education (2019R1A6A3A13095792).

References

[1] Y. Wang, W. Tian, C. Chen, W. Xu, L. Li, Tungsten trioxide nanostructures for photoelectrochemical water splitting: material engineering and charge carrier dynamic manipulation, Adv. Funct. Mater. 29 (2019) 1809036.

[2] S.S. Kalanur, Y.J. Hwang, S.Y. Chae, O.S. Joo, Facile growth of aligned WO_3 nanorods on FTO substrate for enhanced photoanodic water oxidation activity, J. Mater. Chem. A 1 (2013) 3479–3488.

[3] M. Tayebi, A. Tayyebi, B.K. Lee, C.H. Lee, D.H. Lim, The effect of silver doping on photoelectrochemical (PEC) properties of bismuth vanadate for hydrogen production, Sol. Energy Mater. Sol. Cells 200 (2019) 109943.

[4] S.S. Kalanur, I.H. Yoo, J. Park, H. Seo, Insights into the electronic bands of WO_3/$BiVO_4$/TiO_2, revealing high solar water splitting efficiency, J. Mater. Chem. A 5 (2017) 1455–1461.

[5] L. Yang, X. Zhu, S. Xiong, X. Wu, Y. Shan, P.K. Chu, Synergistic $WO_3 \cdot 2H_2O$ nanoplates/WS_2 hybrid catalysts for high-efficiency hydrogen evolution, ACS Appl. Mater. Interfaces 8 (2016) 13966–13972.

[6] M.A. Tekalgne, A. Hasani, D.Y. Heo, Q.V. Le, T.P. Nguyen, T.H. Lee, S.H. Ahn, H.W. Jang, S.Y. Kim, SnO_2@WS_2/p-Si heterostructure photocathode for photoelectrochemical hydrogen production, J. Phys. Chem. C 124 (2020) 647–652.

[7] N. Choudhary, C. Li, H.S. Chung, J. Moore, J. Thomas, Y. Jung, High-performance one-body core/shell nanowire supercapacitor enabled by conformal growth of capacitive 2D WS_2 layers, ACS Nano 10 (2016) 10726–10735.

[8] P. Kumar, M. Singh, G.B. Reddy, Core–shell WO_3–WS_2 nanostructured thin films via plasma assisted sublimation and sulfurization, ACS Appl. Nano Mater. 2 (2019) 1691–1703.

[9] A.J. van der Vlies, G. Kishan, J.W. Niemantsverdriet, R. Prins, Th. Weber, Basic reaction steps in the sulfidation of crystalline tungsten oxides, J. Phys. Chem. B 106 (2002) 3449–3457.

[10] A.J. van der Vlies, R. Prins, Th. Weber, Chemical principles of the sulfidation of tungsten oxides, J. Phys. Chem. B 106 (2002) 9277–9285.

[11] S. Mathuri, M.M. Margoni, K. Ramamurthi, R.R. Babu, V. Ganesh, Hydrothermal assisted growth of vertically aligned platelet like structures of WO_3 films on transparent conducting FTO substrate for electrochromic performance, Appl. Surf. Sci. 449 (2018) 77–91.

[12] N.M. Hung, N.D. Chinh, T.D. Nguyen, E.T. Kim, G.S. Choi, C. Kim, D. Kim, Carbon nanotube-metal oxide nanocomposite gas sensing mechanism assessed via NO_2 adsorption on n-WO_3/p-MWCNT nanocomposites, Ceram. Int. 46 (2020) 29233–29243.

[13] Y. Li, Z. Tang, J. Zhang, Z. Zhang, Defect engineering of air-treated WO_3 and its enhanced visible light-driven photocatalytic and electrochemical performance, J. Phys. Chem. C 120 (2016) 9750−9763.

[14] W. Song, R. Zhang, X. Bai, Q. Jia, H. Ji, Exposed crystal facets of WO_3 nanosheets by phase control on NO_2-sensing performance, J. Mater. Sci.: Mater. Electron. 31 (2020) 610–620.

[15] S. Liu, Y. Zeng, M. Zhang, S. Xie, Y. Tong, F. Cheng, X. Lu, Binder-free WS_2 nanosheets with enhanced crystallinity as a stable negative electrode for flexible asymmetric supercapacitors. J. Mater. Chem. A 5 (2017) 21460–21466.

[16] L. Sharma, P. Kumar, A. Halder, Phase and vacancy modulation in tungsten oxide: electrochemical hydrogen evolution, ChemElectroChem 6 (2019) 3420–3428.

[17] A.A. Mohammad, M. Gillet, Phase transformations in WO_3 thin films during annealing, Thin Solid Films 408 (2002) 302–309.

[18] J.M. Berak, M.J. Sienko, Effect of oxygen-deficiency on electrical transport properties of tungsten trioxide crystals, J. Solid State Chem. 2 (1970) 109–133.

[19] J.W.J. Hamilton, J.A. Byrne, P.S.M. Dunlop, N.M.D. Brown, Photo-oxidation of water using nanocrystalline tungsten oxide under visible light, Int. J. Photoenergy 2008 (2008) 185479.

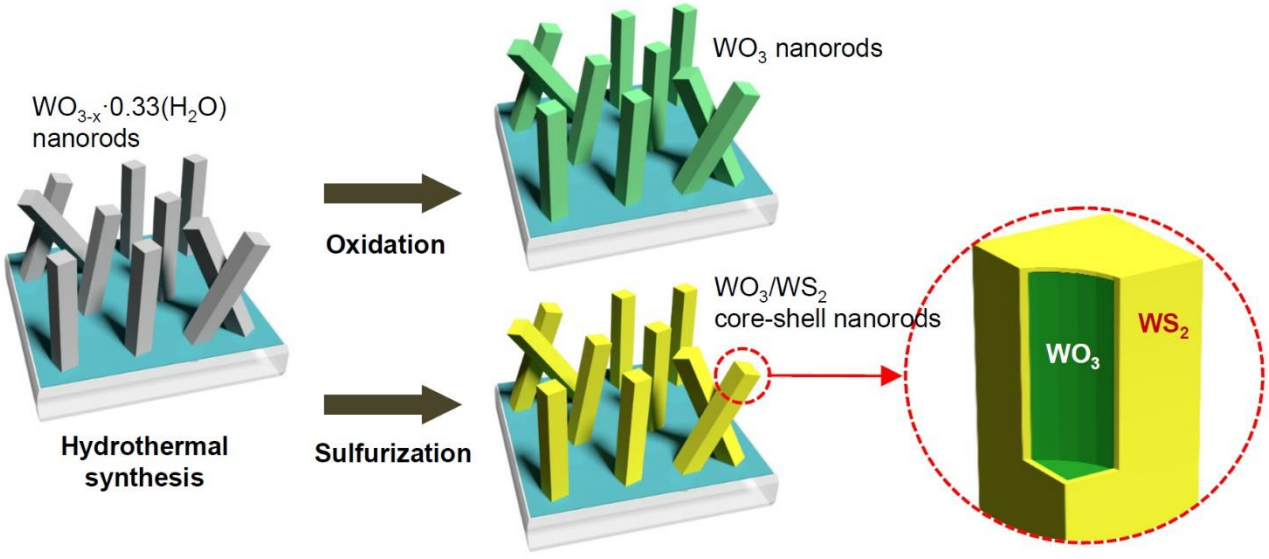

Figure 1. Schematic representation of the syntheses of WO_3 and WO_3/2D WS_2 core–shell nanorods by oxidation and sulfurization of $WO_3 \cdot 0.33H_2O$ nanorods.

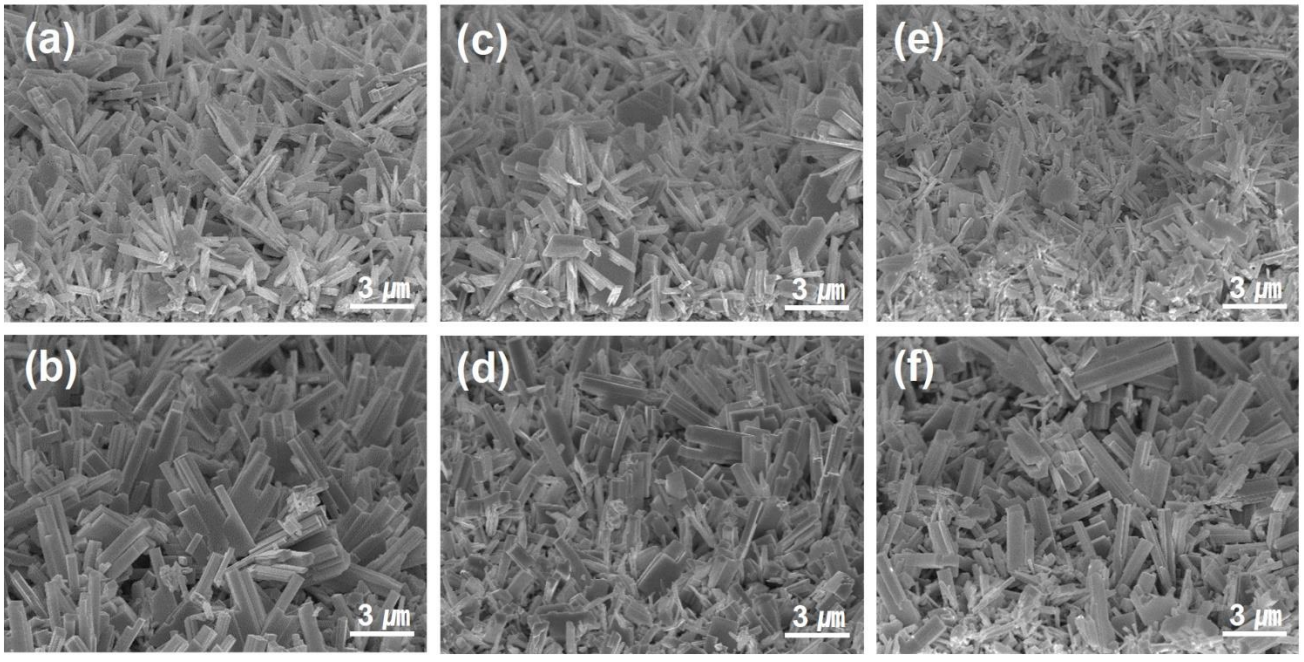

Figure 2. SEM images of (a) W-180, (b) W-200, (c) WO-180, (d) WO-200, (e) WSO-180, and (f) WSO-200.

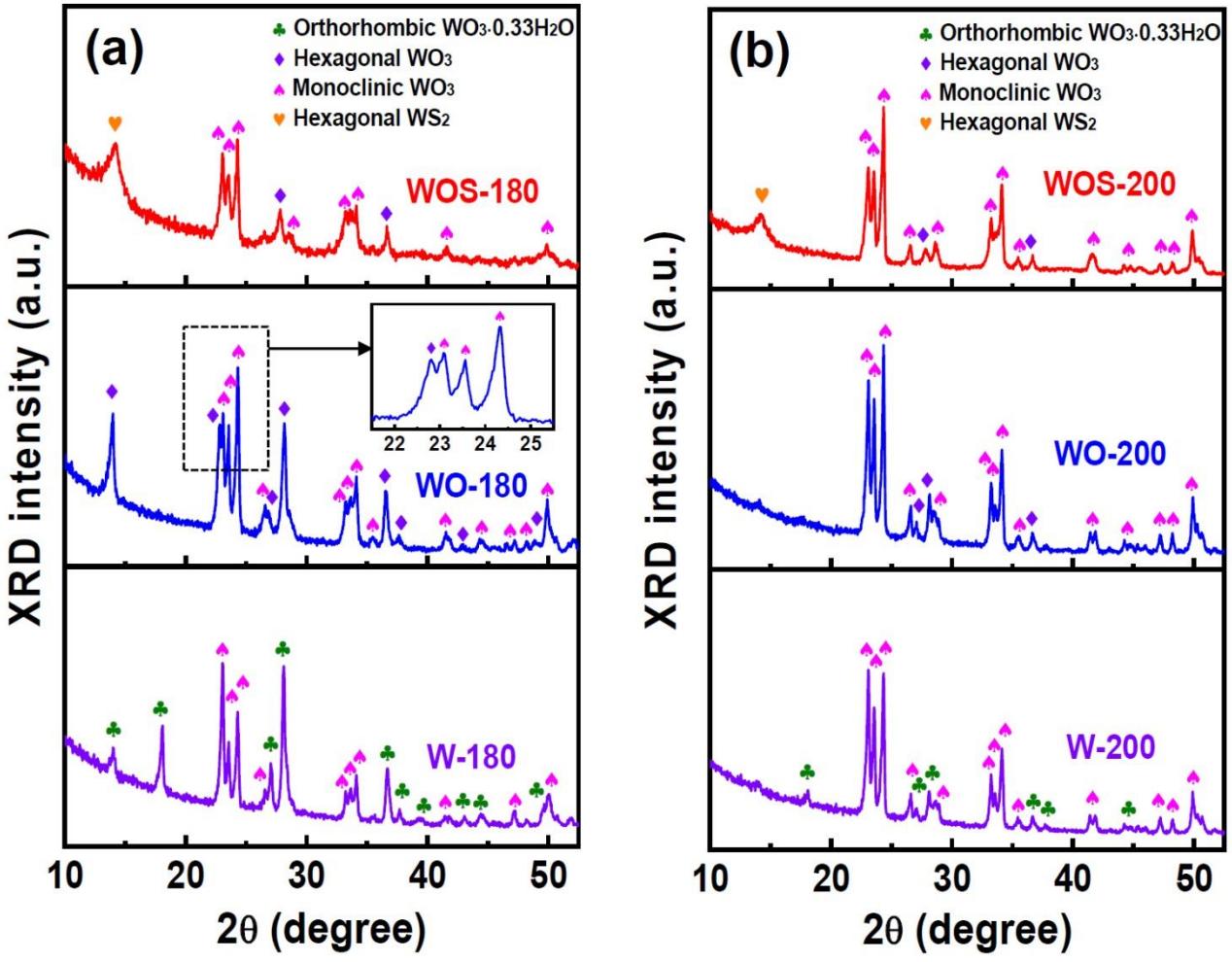

Figure 3. XRD patterns of (a) W-180, WO-180, and WOS-180 and (b) W-200, WO-200, and WOS-200.

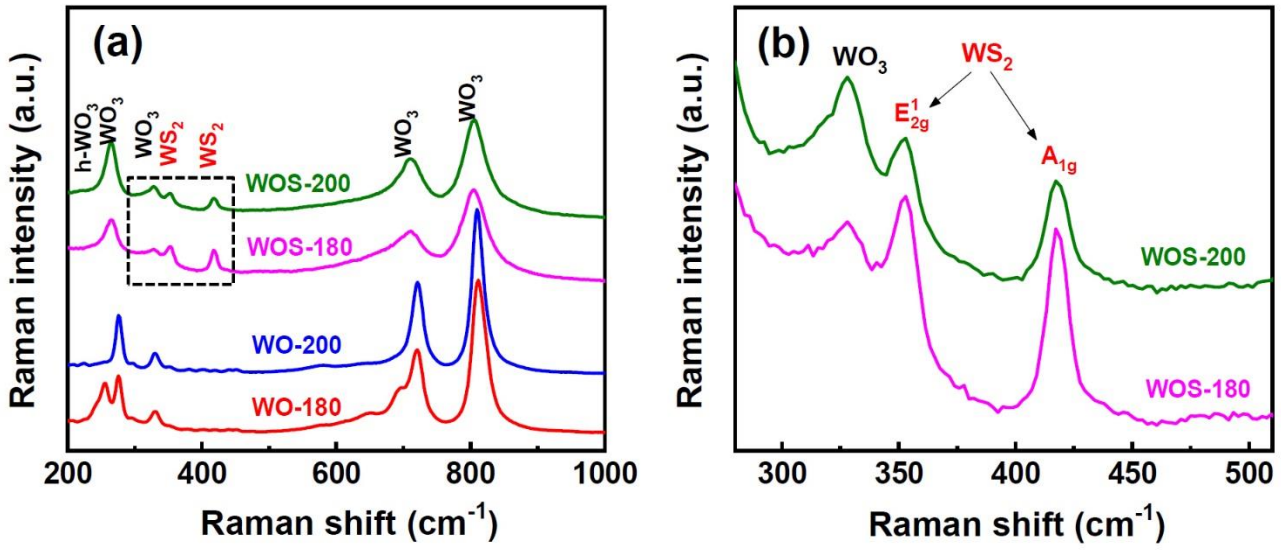

Figure 4. (a) Raman spectra of WO-180, WO-200, WOS-180, and WOS-200. (b) Raman spectra of WOS-180 and WOS-200 corresponding to the dotted box of (a).

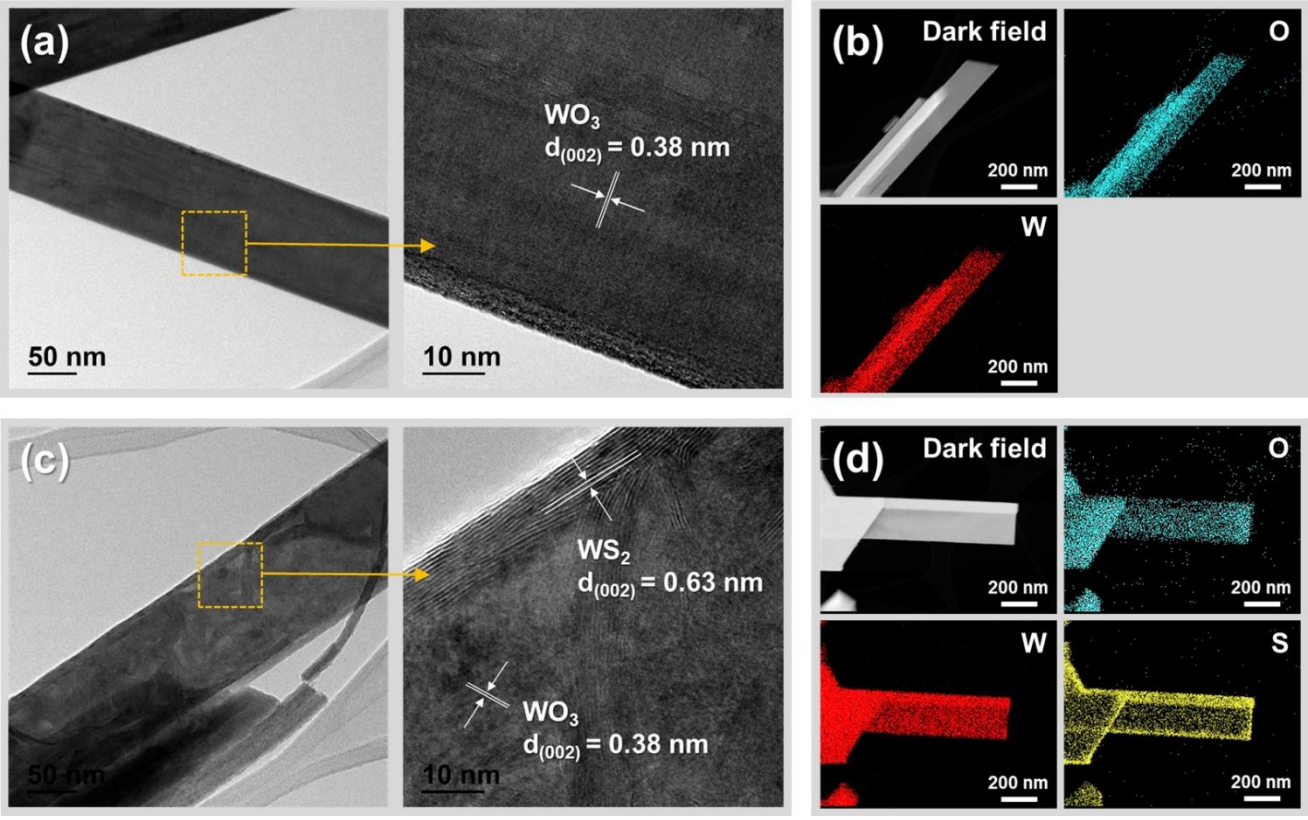

Figure 5. (a) TEM images of WO-200. (b) High-angle annular dark-field and corresponding EDS elemental mapping images of WO-200. (c) TEM images of WSO-200. (d) High-angle annular dark-field and corresponding EDS elemental mapping images of WSO-200.

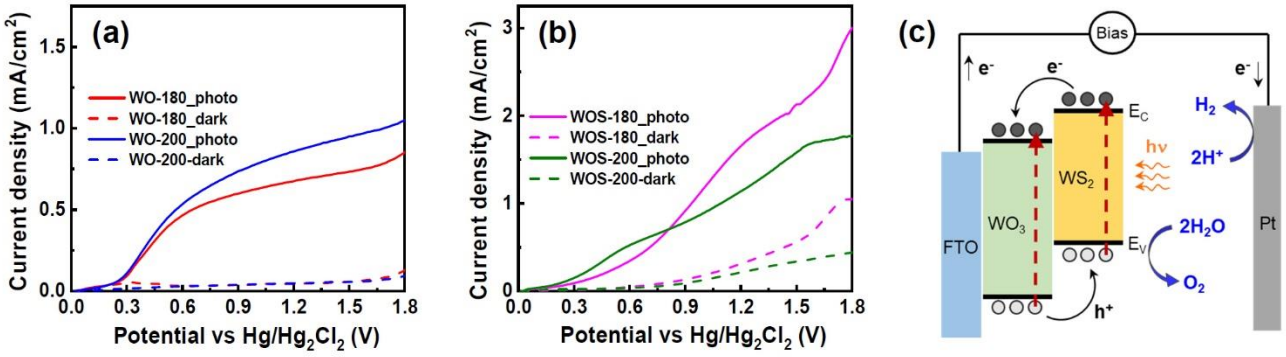

Figure 6. Photo and dark current density–potential curves of PEC cells with various working electrodes: (a) WO-180 and WO-200 and (b) WSO-180 and WSO-200. (c) Schematic of the charge generation and transfer processes in the WO_3/WS_2 heterojunction PEC cell.

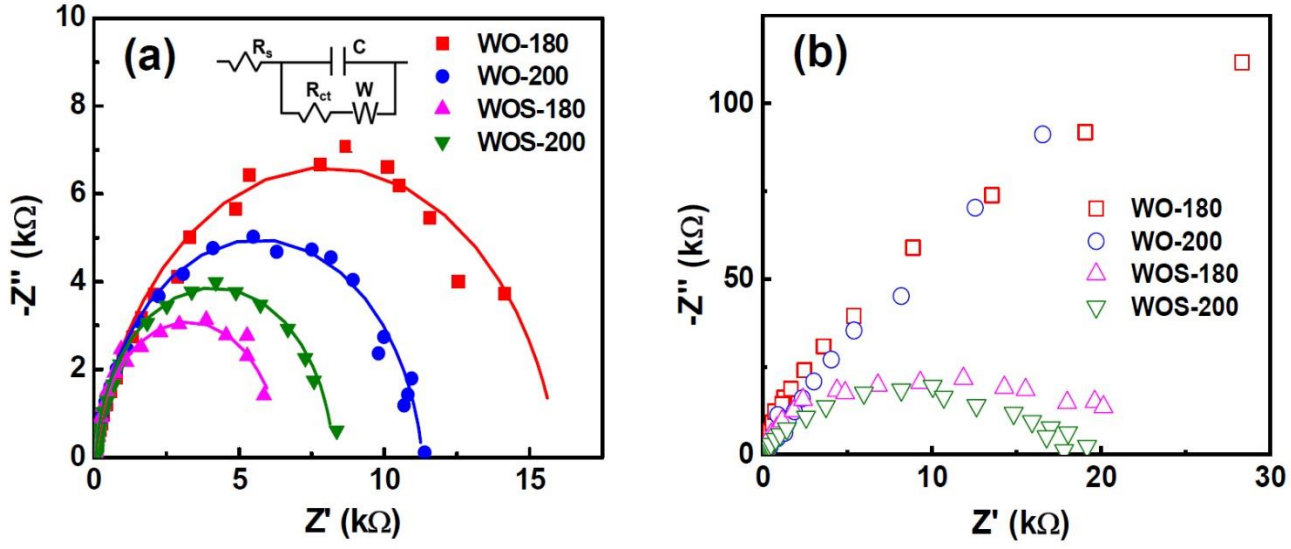

Figure 7. Nyquist plots of WO-180, WO-200, WSO-180, and WSO-200 (a) under illumination and (b) in the dark.

Graphical Abstract

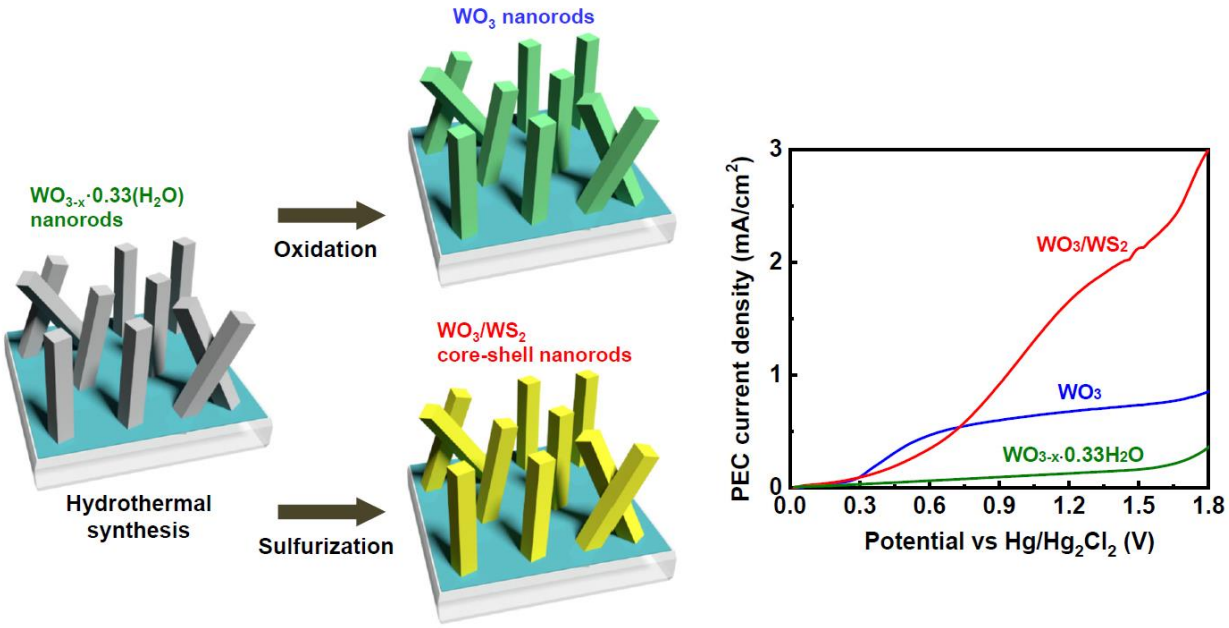

Highlights

- Facile and effective synthesis of 1D WO_3/2D WS_2 core-shell nanorods
- Introducing a novel route to synthesize 2D WS_2 shell layer on WO_3 nanorods utilizing $WO_3 \cdot 0.33H_2O$ phase
- Significantly enhanced photoelectrochemical performance of WO_3/WS_2 core-shell nanorods
- Applicable to various types of heterojunction WO_3/2D WS_2 for photoelectrochemical applications

Declaration of interests

☒ The authors declare that they have no known competing financial interests or personal relationships that could have appeared to influence the work reported in this paper.

☐The authors declare the following financial interests/personal relationships which may be considered as potential competing interests:

Thank you.
Sincerely,

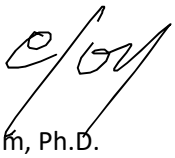

Eui-Tae Kim, Ph.D.
Professor
Department of Materials Science & Engineering
Chungnam National University
Daejeon 34134, Korea
E-mail: etkim@cnu.ac.kr
Tel: +82 42-821-5895